

## Glycomic and Transcriptomic Response of GSC11 Glioblastoma Stem Cells to STAT3 Phosphorylation Inhibition and Serum-Induced Differentiation

Huan He,<sup>†,‡</sup> Carol L. Nilsson,<sup>\*,†,§</sup> Mark R. Emmett,<sup>†,‡</sup> Alan G. Marshall,<sup>†,‡</sup> Roger A. Kroes,<sup>§</sup> Joseph R. Moskal,<sup>§</sup> Yongjie Ji,<sup>||</sup> Howard Colman,<sup>||</sup> Waldemar Priebe,<sup>||</sup> Frederick F. Lang,<sup>||</sup> and Charles A. Conrad<sup>||</sup>

*Ion Cyclotron Resonance Program, National High Magnetic Field Laboratory, Florida State University, Tallahassee, Florida 32310, Department of Chemistry and Biochemistry, Florida State University, Tallahassee, Florida 32306-43903, Falk Center for Molecular Therapeutics, Department of Biomedical Engineering, Northwestern University, Evanston, Illinois 60201, Department of Neuro-oncology, The University of Texas M.D. Anderson Cancer Center, Houston, Texas 77030, and Department of Experimental Therapeutics, The University of Texas M.D. Anderson Cancer Center, Houston, Texas 77030*

Received September 05, 2009

A glioblastoma stem cell (GSC) line, GSC11, grows as neurospheres in serum-free media supplemented with EGF (epidermal growth factor) and bFGF (basic fibroblast growth factor), and, if implanted in nude mice brains, will recapitulate high-grade glial tumors. Treatment with a STAT3 (signal transducer and activator of transcription 3) phosphorylation inhibitor (WP1193) or 10% FBS (fetal bovine serum) both led to a decrease in expression of the stem cell marker CD133 in GSC11 cells, but differed in phenotype changes. Altered glycolipid profiles were associated with some differentially expressed glycogenes. In serum treated cells, an overall increase in glycosphingolipids may be due to increased expression of ST6GALNAC2, a sialyltransferase. Serum treated cells express more phosphatidylcholine (PC), short chain sphingomyelin (SM) and unsaturated long chain phosphatidylinositol (PI). Decrease of a few glycosphingolipids in the STAT3 phosphorylation inhibited cells may be linked to decreased transcripts of ST6GALNAC2 and UGCGL2, a glucosylceramide synthase. A rare 3-sulfoglucuronylparagloboside carrying HNK1 (human natural killer-1) epitope was found expressed in the GSC11 and the phenotypically differentiated cells. Its up-regulation correlates with increased transcripts of a HNK1 biosynthesis gene, B3GAT2 after serum treatment. Taken together with a quantitative phosphoproteomic study of the same GSC line (C. L. Nilsson, et al. *J. Proteome Res.* **2010**, *9*, 430–443), this report represents the most complete systems biology study of cancer stem cell (CSC) differentiation to date. The synergies derived by the combination of glycomic, transcriptomic and phosphoproteomic data may aid our understanding of intracellular and cell-surface events associated with CSC differentiation.

**Keywords:** cancer stem cells • glioma • transcriptomics • glycolipids • phospholipids • metabolomics • FT- ICR MS • 3-sulfoglucuronylparagloboside • lipidomics • HNK1

### Introduction

Cancer stem cells (CSCs),<sup>1</sup> similar to embryonic stem cells (ESCs), possess the abilities of unlimited self-renewal and differentiation to different cell types. Although CSCs constitute only a small percentage (<1%) of the total tumor cell popula-

tion, CSCs present the biggest challenge for treating cancer. CSCs are refractory to traditional cancer therapies such as radiation and chemotherapy that target mature (or differentiated) cancer cells.<sup>1,2</sup> Thus, insights provided by quantitation of metabolomic and transcriptomic responses of CSCs during various differentiation pathways may help to identify new therapeutic targets associated with the stem-like state of CSCs.

\* To whom correspondence should be addressed. E-mail: Carol.Nilsson@pfizer.com.

<sup>†</sup> Ion Cyclotron Resonance Program, National High Magnetic Field Laboratory, Florida State University.

<sup>‡</sup> Department of Chemistry and Biochemistry, Florida State University.

<sup>#</sup> Current address: Pfizer Global Research and Development, 10770 Science Center Dr. (CB2), San Diego, CA 92121.

<sup>§</sup> Northwestern University.

<sup>||</sup> Department of Neuro-oncology, The University of Texas M.D. Anderson Cancer Center.

<sup>||</sup> Department of Experimental Therapeutics, The University of Texas M.D. Anderson Cancer Center.

Altered surface glycosylation patterns on tumor cells are key factors that define tumor malignancy. Overexpression of certain glycans may lead to more invasive and metastatic phenotypes, whereas overexpression of another group of glycans may suppress the growth, invasiveness and metastasis of tumors.<sup>3–5</sup> These glycosylated moieties are present in glycolipids and glycoproteins. Glycosphingolipids (GSLs), abundant in the outer leaflet of the cell membrane, play important roles in cell–cell

## WP1193

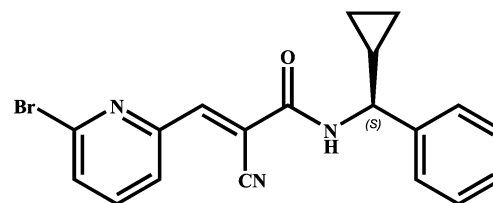


**Figure 1.** Chemical structure of the small molecule STAT3 phosphorylation inhibitor WP1193.

recognition,<sup>6</sup> adhesion,<sup>7</sup> and differentiation.<sup>8</sup> GSLs may cluster “side-by-side” along with sphingomyelin and cholesterol to form a rigid membrane microdomain (lipid raft) or may cluster “head-to-head” through carbohydrates present on adjacent cell membranes. Such microdomains are associated with signal transduction.<sup>4,9,10</sup> Sialyl-Lewis<sup>x</sup> (SLe<sup>x</sup>) and sialyl-Lewis<sup>a</sup> (SLe<sup>a</sup>), tumor-associated antigens presented on the cell surface, are associated with increased cell invasion and metastasis.<sup>11</sup> In various cancer cell lines, coexpression of CD9 and GM3 inhibits invasiveness.<sup>11</sup> Laminin- or fibronectin-dependent cell motility was affected by modified interaction of integrin with CD82 by N-glycosylation in a murine vascular tumor cell line (D14).<sup>12</sup> It was recently reported that in colon cancer stem cells, CD133, a proposed marker for cancer stem cells, possesses an N-terminal region that binds to gangliosides.<sup>13</sup> Thus, cellular ganglioside profiles affect the accessibility of ligands to CD133 and cell–cell interactions involving CD133.

A glioblastoma CSC line, GSC11, was used in this study. GSC11, along with several other glioblastoma CSC lines, was established at M.D. Anderson Cancer Center-Houston from primary gliomas removed from glioma patients.<sup>14</sup> Correctly identifying and isolating CSCs from the nonstem tumor cells was critical for the CSC studies. *In vitro* methods to evaluate CSCs, including the spheroid assay, serial colony-forming unit (CFU), and label-retention assay<sup>15</sup> are generally used for higher throughput.<sup>1,16</sup> For glioma CSC studies, identification and characterization of CSCs involve the use of a neurosphere assay.<sup>17,18</sup> The *in vivo* method to evaluate CSCs is serial transplantation<sup>19</sup> of CSCs in an animal model to demonstrate self-renewal and multicell-type differentiation capabilities.<sup>1</sup>

In the neurosphere assay, collected tumor tissue samples are separated into single cells which are cultured and stimulated with basic fibroblast growth factor (bFGF) and epidermal growth factor (EGF) in a serum-free medium as described in earlier studies.<sup>18,20</sup> Distinct from terminally differentiated tumor cells which tend to adhere to the plate while growing, CSCs grown in suspension culture form free-floating ball-like clusters, or neurospheres. Cultured CSCs express several stem cell markers, including CD133 and nestin. CD133, or prominin-1, is expressed by a variety of stem cells and progenitor cell types<sup>21</sup> and has been used to isolate stem cells or progenitor cells by affinity selection. Singh et al. reported the isolation of CSCs from pediatric brain tumors by CD133 affinity selection,<sup>22</sup> although subsequent studies indicated that CD133 negative cells can also initiate tumors.<sup>23,24</sup>

CSCs are also capable of regenerating tumors that are phenotypically similar to the primary tumor upon differentiation. Differentiation conditions, originally developed for ESCs,<sup>25</sup> employ incubation of CSCs with 10% fetal bovine serum (FBS) for several days. Short-term exposure of glioblastoma CSCs to FBS results in up-regulation of multiple neural lineage markers seen in more differentiated cells, but does not result in terminal differentiation as seen in NSCs (neural stem cells).<sup>26</sup>

Upon incubation with a STAT3 phosphorylation inhibitor, WP1193 (Figure 1),<sup>27</sup> glioblastoma CSCs exhibit cell cycle arrest and reduced self-renewal ability. STAT3 is a member of the signal transducer and activator of transcription (STAT) proteins. Upon activation of phosphorylation by kinases in response to cellular stimuli, STAT3 dimerizes and translocates to the nucleus to modulate the expression of several genes that are involved in cell growth, angiogenesis, immune evasion and apoptosis.<sup>28</sup> STAT3 is regarded as an oncogene, and constitutive

activation of STAT3 has been reported in various types of tumors<sup>29</sup> and glioma CSCs (unpublished data).

We combined chemotherapy, phenotypic response, glycolipidomic, and glycotranscriptomic approaches to investigate the effects of serum-induced differentiation or blockade of STAT3 phosphorylation of glioblastoma cancer stem cells at the molecular level. This report describes the most complete systems biology study of CSC manipulation to date and is instrumental in our ultimate understanding of the mechanisms involved in CSC maintenance and tumorigenicity.

## Experimental Procedures

**Cell Culture Conditions and Treatments.** CSCs were isolated and cultured from glioblastoma tumor(s) that were removed from patients as previously described.<sup>14</sup> GSC11 cells were cultured in 150 mm tissue culture dishes. GSC11 cells were cultured in DMEM-F12 (1:1) media with B27 (Invitrogen, Carlsbad, CA), bFGF (Sigma, St. Louis, MO) and EGF (Sigma, St. Louis, MO) and incubated at 37 °C with 5% CO<sub>2</sub> and 20% O<sub>2</sub>. About 10 million cells each were treated with vehicle control (DMSO), the STAT3 phosphorylation inhibitor (WP1193, 5 μM in DMSO), or 10% fetal bovine serum (Cambrex, East Rutherford, NJ) for 24 h. Collected cells were pelleted at 240g for 5 min at 4 °C and washed twice with HEPES (50 mM, pH 7.0). Three biological replicates (each with three technical replicates) were analyzed.

**Glycotranscriptomics.** The techniques for microarray fabrication, target preparation and data acquisition have been described previously.<sup>30</sup> Briefly, the 359 genes that represented all of the cloned human glycogenes were compiled from NCBI/EMBL/TIGR human sequence databases and the Consortium for Functional Glycomics-CAZy databases (available at [www.cazy.org/](http://www.cazy.org/)). We stringently designed and prioritized individual 45-mer oligonucleotides complementary to sequences within these human mRNAs as well as control oligonucleotides representing the most traditionally accepted and commonly utilized housekeeping genes<sup>31</sup> (with ArrayDesigner v2.03). The optimal oligonucleotides were individually synthesized with the addition of a 5'-amino linker (C6-TFA, Glen Research, Sterling, VA) onto each oligonucleotide, then robotically arrayed and covalently linked in quadruplicate to aldehyde-coated glass microscope slides, and quality controlled prior to use. Total RNA was extracted from tissues with guanidine isothiocyanate and CsCl-ultracentrifugation, purified (Qiagen, Valencia, CA) and used as the substrate for RNA amplification and labeling, exactly as described.<sup>30</sup> Universal human reference RNA (Stratagene, La Jolla, CA) was used in the analyses and identical aliquots were treated concurrently with control samples. Equivalent amounts of Cy5-labeled (experimental) and purified Cy3-labeled (reference) amplified RNA (aRNA) targets (each labeled to 15–18% incorporation) were combined, denatured and hybridized at

46 °C for 16 h. Following sequential high-stringency washes, individual Cy3 and Cy5 fluorescence hybridization to each spot on the microarray was quantitated by a ScanArray 4000XL high resolution confocal laser scanner (Packard Bioscience, Meriden, CT). Arrays were scanned (at 633 and 543 nm) at 5  $\mu$ m resolution by use of QuantArray software [v3.0] at the maximal laser power that produced no saturated spots. The adaptive threshold method was used to differentiate the spot from the background and spot intensity determined from median pixel intensity. Prior to normalization, eight individual quality confidence measurements were calculated for each scanned array and spots were flagged that did not pass stringent selection criteria. The data from each channel were normalized with the LOWESS curve-fitting equation on a print-tip specific basis (GeneTraffic v2.8, Iobion Informatics, La Jolla, CA). The experiments were performed in triplicate on three biological replicates.

**Quantitative Real-Time Polymerase Chain Reaction (qRT-PCR).** The expression levels of selected genes were analyzed by real-time PCR by use of Brilliant SYBR Green qRT-PCR Master Mix (Stratagene) on an Mx3000P Real-Time PCR System (Stratagene, La Jolla, CA). Reverse transcription of 1  $\mu$ g of DNased, total RNA was primed with oligo(dT) and random hexamers and was performed exactly as described.<sup>32</sup> All primer sets were designed across intron/exon boundaries to derive ~100 bp amplicons, with individual primer concentrations and final amplification conditions optimized for each gene. The primers used in this study were B3GAT2 (forward) 5'-AAACG-GCAAAGTTGTTGG-3', B3GAT2 (reverse) 5'-TGACTTGAAGACT-TACAGCA-3', NEU3 (forward) 5'-CAGAGAACGTTCTACGA-3', NEU3 (reverse) 5'-CTTCCATCAGTGGCTTCAG-3', ST6GALNAC2 (forward) 5'-CTGAGATCGGCCATTCTG-3', ST6GALNAC2 (reverse) 5'-TGTAGCAGCTTGAATTACTGG-3', NEU1 (forward) 5'-CTTCTTCTCCAACCCAGCA-3', NEU1 (reverse) 5'-GACTGTCTC-TTCCGCCA-3', UGCGL2 (forward) 5'-TCTCAGTCAAGATC-CAAACAG-3', UGCGL2 (reverse) 5'-GTTTCACACCACAGCCAG-3'. Dissociation curves were performed on all reactions to ensure product purity. Original input RNA amounts were calculated by comparison to standard curves by use of purified PCR product as a template for the mRNAs of interest and were normalized to amount of cDNA content. Triplicate PCR experiments were performed on each of three biological replicates for each treatment group.

**Polar Lipid Extraction.** Polar lipids were extracted as previously described.<sup>33–35</sup> Briefly, cells (~2  $\times$  10<sup>6</sup>) were lysed by the addition of methanol/chloroform (1:1, v/v) and the mixture was sonicated for 30 min followed by incubation at 48 °C overnight to optimize polar lipid yield. The supernatant was collected and partitioned with additional chloroform:H<sub>2</sub>O (4:11, v/v) after centrifugation. The upper aqueous layer containing polar lipids was collected, dried and stored in a nitrogen atmosphere. Approximately 1/50 of the total polar lipid extract was consumed per nanoliquid chromatography (nLC) MS experiment which allowed for multiple analytical replicate studies.

**Polar Lipid Nano-LC-MS.** The previously reported nLC-MS procedure of polar lipid analysis<sup>33,34</sup> was slightly modified in the current study. The polar lipid fraction was redissolved in 80% methanol (aq) containing 10 mM NH<sub>4</sub>OAc and separated by nLC (Eksigent 1D system, Livermore, CA) in an 80 mm  $\times$  50  $\mu$ m column (New Objective, Woburn, MA) with self-packed phenyl-hexyl resin (Phenomenex, Torrance, CA). The gradient was 17%/83% to 2%/98% A/B for 15 min and isocratic at 2%/98% A/B for another 12 min (Solvent A, 98%/2% H<sub>2</sub>O/methanol

with 10 mM NH<sub>4</sub>OAc; B, 98%/2% methanol/H<sub>2</sub>O with 10 mM NH<sub>4</sub>OAc) at a flow rate of 550 nL/min. nLC-effluent was online analyzed by negative-ion microelectrospray<sup>36,37</sup> into a modified hybrid LTQ 14.5 T FT-ICR MS.<sup>38,39</sup> Negative-ion microelectrospray was chosen over positive-ion mode for better S/N ratio of analyzed polar lipids.<sup>40</sup> Automatic gain control (AGC) was set at 1 million ions in the ICR cell. Precursor ion mass spectra were collected at high mass resolving power ( $m/\Delta m_{50\%} = 200\ 000$  at  $m/z$  400) and repetition rate >1 Hz. Typical broadband external calibration mass accuracy was better than 500 ppb. Data-dependent tandem mass spectrometry by collisional induced dissociation (CID) was performed in the linear ion trap during collection of the ICR time domain data. Data was analyzed manually. Average signal magnitudes as well as standard deviation from two biological replicates (each with three technical replicates) were calculated for differential analysis of glycolipids or phospholipids among samples. Ratio of expression levels of glycolipids and phospholipids as well as standard deviation among samples were calculated from the above-mentioned average signal magnitudes.

## Results

**Glycotranscriptomics.** Of the 359 glycogenes evaluated, 23 genes exhibited statistically significant expression differences between the FBS-treated and control cultures (Table 1) and 35 genes exhibited statistically significant differences between the WP1193-treated and control cultures (Table 2). Significantly changed expression was identified for transcripts of ST6 ( $\alpha$ -N-acetyl-neuraminy-2,3- $\beta$ -galactosyl-1,3)-N-acetylgalactosaminide  $\alpha$ 2,6-sialyltransferase (ST6GALNAC2), UDP-glucose ceramide glucosyltransferase-like 2 (UGCGL2), phosphatidylinositol glycan (PIGA) and UDP glucuronosyltransferase 2, polypeptide A1 (UGT2A1) following FBS treatment and in ST6 ( $\alpha$ -N-acetyl-neuraminy-2,3- $\beta$ -galactosyl-1,3)-N-acetylgalactosaminide  $\alpha$ 2,6-sialyltransferase 4 (ST6GALNAC4) and sialidase 3 (NEU3) following WP1193 treatment. Changes in glycogene expression identified in FBS-induced phenotypic differentiation included increases in transcripts related to proteoglycan deposition and ECM remodeling, including  $\beta$ 1, 3-glucuronyltransferase 2 (B3GAT2), and UDP-glucose ceramide glucosyltransferase-like 2 (UGCGL2). WP1193-mediated inhibition of STAT3 had little effect on extracellular matrix-related genes, and the predominant effect was increased expression of genes responsible for protein N- and O-linked glycosylation. Key genes identified in WP1193 treated GSC11 cultures were dolichyl-phosphate mannose-transferase polypeptide 1 (DPM1), asparagine-linked glycosylation 5 homologue (dolichyl-phosphate  $\beta$ -glucosyltransferase) (ALG5), asparagine-linked glycosylation 14 homologue (ALG14), mannosyl ( $\alpha$ 1,3-)-glycoprotein  $\beta$ 1,4-N-acetylglucosaminyltransferase, isozyme b (MGAT4B),  $\alpha$ -mannosidase, class 1b, member 1 (MAN1B1), UDP-n-acetyl- $\alpha$ -D-galactosamine:polypeptide N-acetylgalactosaminyltransferase-like 4 (GALNT4), UDP-GlcNAc: $\beta$ -gal  $\beta$ 1,3-N-acetylglucosaminyltransferase 3 (B3GNT3), and fucosyltransferase 7 ( $\alpha$ 1,3 fucosyltransferase) (FUT7).

**qRT-PCR Corroboration of the Microarray Data.** We chose five glycogenes that have not been previously associated with differentiation of glioblastoma stem cells and measured mRNA levels by real-time quantitative RT-PCR (Figure 2). Our approach to transcriptome profiling was to use the focused microarrays as a screening tool to identify statistically significant differentially expressed genes followed by corroboration

**Table 1.** FBS-Associated Transcripts Identified by Microarray Analysis (at <5% FDR)<sup>a</sup>

<i>GENBANK Accession</i>	<i>Fold Change<sup>b</sup></i>	<i>p-value</i>	<i>Gene ID</i>
<b>BLOOD GROUP GLYCOLIPID BIOSYNTHESIS LACTOSERIES</b>			
NM_020121	<b>1.11</b>	2.49	UDP-GLUCOSE CERAMIDE GLUCOSYLTRANSFERASE-LIKE 2 (UGCGL2)
<b>GLOBOSIDE METABOLISM</b>			
NM_021996	<b>1.11</b>	0	GLOBOSIDE α1,3-N-ACETYLGLACTOSAMINYLTRANSFERASE 1 (GBGT1)
NM_003781	<b>1.37</b>	0	UDP-GAL:βGlcNAc β1,3-GALACTOSYLTRANSFERASE, POLYPEPTIDE 3 (B3GALNT1)
<b>GLYCOLYSIS/GLUCONEOGENESIS</b>			
NM_000188	<b>-1.34</b>	0	HEXOKINASE 1
NM_002046	<b>-1.21</b>	0	GLYCERALDEHYDE-3-PHOSPHATE DEHYDROGENASE (GAPDH)
NM_001428	<b>-1.11</b>	0	α-ENOLASE 1 (ENO3)
<b>N GLYCAN BIOSYNTHESIS</b>			
NM_005787	<b>1.12</b>	0	ASPARAGINE-LINKED GLYCOSYLATION 3 HOMOLOG (α1,3-MANNOSYLTRANSFERASE) (ALG3)
NM_019109	<b>-1.11</b>	1	ASPARAGINE-LINKED GLYCOSYLATION 1 HOMOLOG (YEAST, β1,4-MANNOSYLTRANSFERASE) (ALG1)
NM_054013	<b>-1.11</b>	0	MANNOSYL (α1,3)-GLYCOPROTEIN β1,4-N-ACETYLGLUCOSAMINYLTRANSFERASE, ISOZYME B (MGAT4B)
<b>N GLYCAN DEGRADATION</b>			
NM_000434	<b>1.11</b>	0	SIALIDASE 1 (NEU1)
NM_000528	<b>1.11</b>	0	α-MANNOSIDASE, CLASS 2B, MEMBER 1 (MAN2B1)
NM_032020	<b>-1.16</b>	0	FUCOSIDASE, α-L-2 (FUCA2)
<b>O GLYCAN BIOSYNTHESIS</b>			
NM_022087	<b>1.16</b>	0	UDP-N-ACETYL-α-D-GALACTOSAMINE:POLYPEPTIDE N-ACETYLGLACTOSAMINYLTRANSFERASE 11 (GALNT11)
NM_017423	<b>-1.19</b>	0	UDP-N-ACETYL-α-D-GALACTOSAMINE:POLYPEPTIDE N-ACETYLGLACTOSAMINYLTRANSFERASE 7 (GALNT7)
NM_004751	<b>1.10</b>	0	GLUCOSAMINYL (N-ACETYL) TRANSFERASE 3, MUCIN TYPE (GCNT3)
<b>OTHER (glyco-related)</b>			
NM_018446	<b>1.14</b>	0	GLYCOSYLTRANSFERASE 8 DOMAIN CONTAINING 1 (GLT8D1)
NM_006798	<b>1.11</b>	0.96	UDP GLUCURONOSYLTRANSFERASE 2 FAMILY, POLYPEPTIDE A1 (UGT2A1)
NM_080742	<b>1.11</b>	0	β1,3-GLUCURONYLTRANSFERASE 2 (B3GAT2)
NM_006456	<b>1.11</b>	2.49	ST6 (α-N-ACETYL-NEURAMINYL-2,3-β-GALACTOSYL-1,3)-N-ACETYLGLACTOSAMINIDE α2,6-SIALYLTRANSFERASE (ST6GALNAC2)
NM_004000	<b>1.11</b>	0	CHITINASE 3-LIKE 2 (CHI3L2)
NM_001276	<b>1.10</b>	4.97	CHITINASE 3-LIKE 1 (CHI3L1)
NM_000642	<b>-1.13</b>	0	AMYLO-1, 6-GLUCOSIDASE, 4-α-GLUCANOTRANSFERASE (AGL)
NM_024656	<b>-1.11</b>	0	GLYCOSYLTRANSFERASE 25 DOMAIN CONTAINING 1 (GLT25D1)
<b>OTHER (housekeeping)</b>			
NM_000996	<b>1.37</b>	0	RIBOSOMAL PROTEIN L35A (RPL35A)
NM_000972	<b>1.35</b>	0	RIBOSOMAL PROTEIN L7A (RPL7A)
NM_005252	<b>1.24</b>	0	V-FOS FB1 MURINE OSTEOSARCOMA VIRAL ONCOGENE HOMOLOG (FOS)
NM_000602	<b>1.23</b>	0	SERPIN PEPTIDASE INHIBITOR, CLADE E (NEXIN, PLASMINOGEN ACTIVATOR INHIBITOR TYPE 1), MEMBER 1 (SERPINE1)
NM_007096	<b>1.23</b>	0	CLATHRIN, LIGHT POLYPEPTIDE (CLTA)
NM_002107	<b>1.20</b>	0	H3 HISTONE, FAMILY 3A (H3F3B)
NM_005594	<b>1.19</b>	0	NASCENT-POLYPEPTIDE-ASSOCIATED COMPLEX ALPHA POLYPEPTIDE (NACA)
NM_001540	<b>1.17</b>	0	HEAT SHOCK 27KDA PROTEIN 1 (HSPB1)
NM_000546	<b>1.16</b>	0	TUMOR PROTEIN P53 (TP53)
AB037787	<b>1.15</b>	0	NEUROLIGIN 2 (NLGN2)
NM_006923	<b>1.14</b>	0	STROMAL CELL-DERIVED FACTOR 2 (SDF2)
NM_005324	<b>1.13</b>	0.96	H3 HISTONE, FAMILY 3A (H3F3B)
NM_002290	<b>1.13</b>	0	α4 LAMININ (LAMA4)
NM_004046	<b>1.13</b>	0	ATP SYNTHASE, H <sup>+</sup> TRANSPORTING, MITOCHONDRIAL F1 COMPLEX, ? SUBUNIT 1 (ATP5A1)
NM_003380	<b>1.12</b>	0	VIMENTIN (VIM)
NM_003877	<b>1.12</b>	0	SUPPRESSOR OF CYTOKINE SIGNALING 2 (SOCS2)
NM_015831	<b>1.12</b>	0	ACETYLCHOLINESTERASE (ACHE)
BC029126	<b>1.12</b>	0.96	HYPOTHETICAL PROTEIN LOC129530 (LYG1)
BC014495	<b>1.11</b>	0	RADICAL FRINGE HOMOLOG (DROSOPHILA) (RFNG)
NM_003472	<b>-1.32</b>	0	DEK ONCOGENE (DEK)
NM_006082	<b>-1.28</b>	0	α-TUBULIN (TUBA1C)
NM_002156	<b>-1.20</b>	0	HEAT SHOCK 60KDA PROTEIN 1 (HSPD1)
NM_001101	<b>-1.20</b>	0	β-ACTIN (ACTB)
NM_005348	<b>-1.17</b>	0	HEAT SHOCK PROTEIN 90KDA ALPHA, CLASS A MEMBER 1 (HSP90AA1)
NM_001440	<b>-1.14</b>	0	EXOSTOSES (MULTIPLE)-LIKE 3 (EXTL3)
NM_000194	<b>-1.14</b>	3.18	HYPOXANTHINE PHOSPHORIBOSYLTRANSFERASE 1 (HPRT1)
NM_007355	<b>-1.13</b>	0	HEAT SHOCK PROTEIN 90KDA ALPHA, CLASS B MEMBER 1 (HSP90AB1)
NM_002014	<b>-1.11</b>	0	FK506 BINDING PROTEIN 4 (FKBP4)
NM_002641	<b>-1.11</b>	4.97	PHOSPHATIDYLINOSITOL GLYCAN, CLASS A (PIGA)
NM_004455	<b>-1.11</b>	4.97	EXOSTOSES (MULTIPLE)-LIKE 1 (EXTL1)
NM_001759	<b>-1.10</b>	0	CYCLIN D2 (CCND2)

<sup>a</sup> Altered expression of glycogenes between 10% FBS treated and control GSC11 cells. <sup>b</sup> The fold change was calculated between mean values of GSC11 cells + FBS (*n* = 3) and control GSC11 cells (*n* = 3). Positive values indicate an increase, and negative a decrease, in gene expression in GSC11 + FBS relative to control GSC11.

of a subset of these based on higher throughput methodologies, including quantitative qRT-PCR. cDNA input was chosen as a reference because the expression of the majority of the prototypical housekeeping genes was affected during the different differentiation protocols. Consistent with the microarray data, we measured significant up-regulation of B3GAT2 in both the FBS- and WP1193-treated cells (Figure 2D). We also observed significant up-regulation of ST6GALNAC2 in the FBS-treated cells (Figure 2E). There were no significant differences in sialidase expression (either NEU1 or NEU2) observed (Figure 2B,C). Statistically significantly decreased expression of UGCGL2 was also measured in both the FBS- and WP1193-treated cells (Figure 2A).

**Glycolipids.** Nano-LC separation of glycolipids from complex cell extract mixtures prior to MS detection was crucial for enhanced sensitivity.<sup>33</sup> Each nLC-MS experiment used only 1/50 (approximately) of the polar lipid fraction of cells extract (~2 × 10<sup>6</sup>). Cellular polar lipids were reasonably resolved chromatographically based on variations of oligosaccharide and aglycone moieties. Separation prior to MS detection of complex mixture components with different ionization efficiencies and/or abundance improves sensitivity, dynamic range and quantification linearity. Signal magnitude and accurate mass measurement of the precursor ions from LC effluent were provided by 14.5 T FT-ICR MS.<sup>38,39</sup> Accurate mass (typically better than 1 ppm), LC retention time trends, along with available tandem

**Table 2.** WP1193-Associated Transcripts Identified by Microarray Analysis (at <5% FDR)<sup>a</sup>

<i>GENBANK Accession</i>	<i>Fold Change<sup>b</sup></i>	<i>q-value</i>	<i>Gene ID</i>
<b>BLOOD GROUP GLYCOLIPID BIOSYNTHESIS LACTOSERIES</b>			
NM_000149	1.14	0	FUCOSYLTRANSFERASE 3 (GALACTOSIDE 3(4)-L-FUCOSYLTRANSFERASE, LEWIS BLOOD GROUP) (FUT3)
NM_020121	-1.11	4.84	UDP-GLUCOSE CERAMIDE GLUCOSYLTRANSFERASE-LIKE 2 (UGCGL2)
<b>GANGLIOSIDE BIOSYNTHESIS</b>			
NM_014403	-1.15	0	ST6 (α-N-ACETYL-NEURAMINYL-2,3-β-GALACTOSYL-1,3)-N-ACETYLGLUCOSAMINIDE α2,6-SIALYLTRANSFERASE 4 (ST6GALNAC4)
<b>GLOBOSIDE METABOLISM</b>			
NM_000521	-1.11	0	HEXOSAMINIDASE B (BETA POLYPEPTIDE) (HEXB)
NM_003781	1.25	0	UDP-GAL-β-GLCNAC β1,3-GALACTOSYLTRANSFERASE, POLYPEPTIDE 3 (B3GALNT1)
NM_004751	1.14	0	GLUCOSAMINYL (N-ACETYL) TRANSFERASE 3, MUCIN TYPE (GCNT3)
NM_033168	-1.14	0	UDP-GAL-β-GLCNAC β1,3-GALACTOSYLTRANSFERASE, POLYPEPTIDE 3 (B3GALNT1)
<b>GLYCOLYSIS/GLUCONEOGENESIS</b>			
NM_000188	-1.27	0	HEXOKINASE 1 (HK1)
NM_002629	-1.11	0	PHOSPHOGLYCERATE MUTASE 1 (BRAIN) (PGAM1)
<b>GLYCOSAMINOGLYCAN DEGRADATION</b>			
NM_025191	-1.22	0	DKFZP434N126 PROTEIN (EDEM3)
<b>N GLYCAN BIOSYNTHESIS</b>			
NM_003859	1.19	0	DOLICHYL-PHOSPHATE MANNOSYLTRANSFERASE POLYPEPTIDE 1 (DPM1)
NM_013338	1.10	0	ASPARAGINE-LINKED GLYCOSYLATION 5 HOMOLOG (YEAST, DOLICHYL-PHOSPHATE β-GLUCOSYLTRANSFERASE) (ALG5)
NM_144988	1.18	0	ASPARAGINE-LINKED GLYCOSYLATION 14 HOMOLOG (YEAST) (ALG14)
NM_054013	-1.29	0	MANNOSYL (α1,3)-GLYCOPROTEIN β1,4-N-ACETYLGLUCOSAMINYLTRANSFERASE, ISOZYME B (MGAT4B)
NM_007230	-1.14	0	α-MANNOSIDASE, CLASS 1B, MEMBER 1 (MAN1B1)
<b>N GLYCAN DEGRADATION</b>			
NM_000434	1.14	0	SIALIDASE 1 (LYSOSOMAL SIALIDASE) (NEU1)
NM_006656	1.11	0	SIALIDASE 3 (MEMBRANE SIALIDASE) (NEU3)
NM_005908	1.10	1.82	β-MANNOSIDASE A, LYSOSOMAL
<b>O GLYCAN BIOSYNTHESIS</b>			
BC037341	1.15	0	UDP-N-ACETYL-α-D-GALACTOSAMINE:POLYPEPTIDE N-ACETYLGLUCOSAMINYLTRANSFERASE-LIKE 4 (GALNT4)
NM_022479	-1.11	1.34	WILLIAMS-BEUREN SYNDROME CHROMOSOME REGION 17 (WBSR17)
NM_014256	1.14	0	UDP-GLCNAC:β-GAL β1,3-N-ACETYLGLUCOSAMINYLTRANSFERASE 3 (B3GNT3)
NM_004479	1.10	2.66	FUCOSYLTRANSFERASE 7 (α1,3-FUCOSYLTRANSFERASE) (FUT7)
<b>OTHER (glyco-related)</b>			
NM_005328	1.14	0	HYALURONAN SYNTHASE 2 (HAS2)
NM_004000	1.14	0	CHITINASE 3-LIKE 2 (CHI3L2)
NM_006798	1.13	0	UDP GLUCURONOSYLTRANSFERASE 2 FAMILY, POLYPEPTIDE A1 (UGT2A1)
NM_014918	1.12	0	CHONDROITIN SYNTHASE 1 (CHSY1)
NM_000644	1.12	1.34	AMYO-1, 6-GLUCOSIDASE, 4-α-GLUCANOTRANSFERASE (AGL)
NM_080742	1.11	0	β1,3-GLUCURONYLTRANSFERASE 2 (GLUCURONOSYLTRANSFERASE S) (B3GAT2)
NM_018371	1.10	2.66	CHONDROITIN β1,4-N-ACETYLGLUCOSAMINYLTRANSFERASE (CHGN)
NM_020472	1.10	1.82	PHOSPHATIDYLINOSITOL GLYCAN, CLASS A (PIGA)
NM_133642	-1.15	4.29	LIKE-GLYCOSYLTRANSFERASE (LARGE)
NM_022167	-1.13	0	XYLOSYLTRANSFERASE II (XYLT2)
NM_001076	-1.12	1.34	UDP GLUCURONOSYLTRANSFERASE 2 FAMILY, POLYPEPTIDE B15 (UGT2B15)
NM_033158	-1.11	0	HYALURONOGLUCOSAMINIDASE 2 (HYAL2)
NM_152932	-1.10	0	GLYCOSYLTRANSFERASE 8 DOMAIN CONTAINING 1 (GLT8D1)
<b>OTHER (housekeeping)</b>			
NM_001540	1.80	0	HEAT SHOCK 27KDA PROTEIN 1 (HSPB1)
NM_000602	1.47	0	SERPIN PEPTIDASE INHIBITOR, CLADE E (NEXIN, PLASMINOGEN ACTIVATOR INHIBITOR TYPE 1), MEMBER 1
NM_002394	1.30	0	SOLUTE CARRIER FAMILY 3 (ACTIVATORS OF DIBASIC AND NEUTRAL AMINO ACID TRANSPORT), MEMBER 2
NM_002156	1.26	0	HEAT SHOCK 60KDA PROTEIN 1 (HSPD1)
NM_005348	1.25	0	HEAT SHOCK PROTEIN 90KDA ALPHA, CLASS A MEMBER 1 (HSP90AA1)
AB037784	1.19	0	ARYLACETAMIDE DEACETYLASE-LIKE 1 (AADACL1)
NM_005252	1.19	0	V-FOS FB MURINE OSTEOSARCOMA VIRAL ONCOGENE HOMOLOG (FOS)
NM_000239	1.17	0	LYSOZYME (LYZ)
NM_005345	1.15	0	HEAT SHOCK 70KDA PROTEIN 1A (HSPA1B)
NM_005324	1.15	0	H3 HISTONE, FAMILY 3A (H3F3B)
NM_002425	1.15	0	MATRIX METALLOPEPTIDASE 10 (MMP10)
NM_003380	1.14	0	VIMENTIN (VIM)
NM_001537	1.13	0	HEAT SHOCK FACTOR BINDING PROTEIN 1 (HSBP1)
NM_000996	1.12	4.29	RIBOSOMAL PROTEIN L35A (RPL35A)
NM_002405	1.11	0	MANIC FRINGE HOMOLOG (DROSOPHILA) (MFNG)
NM_002107	1.11	0	H3 HISTONE, FAMILY 3A (H3F3B)
NM_025092	1.11	0	ATH1, ACID TREHALASE-LIKE 1 (YEAST) (ATH1)
NM_173847	1.11	0.75	SPERM ACROSOME ASSOCIATED 3 (SPACA3)
NM_003472	-1.35	0	DEK ONCOGENE (DEK)
NM_001428	-1.31	0	α-ENOLASE 1 (ENO3)
NM_018136	-1.23	0	HYPOTHETICAL PROTEIN FLJ10517 (ASPM)
NM_004046	-1.20	0	ATP SYNTHASE, H <sup>+</sup> TRANSPORTING, MITOCHONDRIAL F1 COMPLEX, α SUBUNIT 1 (ATP5A1)
NM_005573	-1.16	1.82	LAMIN B1 (LMNB1)
NM_006082	-1.16	1.34	α-TUBULIN (TUBA1C)
AF112219	-1.16	0	ESTERASE D/FORMYLGLUTATHIONE HYDROLASE (ESD)
NM_001440	-1.13	0	EXOSTOSIN (MULTIPLE)-LIKE 3 (EXTL3)
NM_020742	-1.13	0	NEUROGIN 4, X-LINKED (NLGN4X)
NM_005228	-1.13	0	EPIDERMAL GROWTH FACTOR RECEPTOR (EGFR)
NM_001618	-1.12	0	POLY (ADP-RIBOSE) POLYMERASE FAMILY, MEMBER 1 (PARP1)
NM_173087	-1.12	0	CALPAIN 3 (CAPN3)
NM_006572	-1.11	1.34	GUANINE NUCLEOTIDE BINDING PROTEIN (G PROTEIN), ALPHA 13 (GNA13)
NM_002103	-1.11	2.75	GLYCOGEN SYNTHASE 1 (MUSCLE) (GYS1)

<sup>a</sup> Altered expression of glycogenes between WP1193 treated and control GSC11 cells. <sup>b</sup> The fold change was calculated between mean values of GSC11 cells + WP1193 (*n* = 3) and control GSC11 cells (*n* = 3). Positive values indicate an increase, and negative a decrease, in gene expression in GSC11 + WP1193 relative to control GSC11.

mass spectra generated from collisional induced dissociation (CID) of precursor ions in the linear ion trap (LTQ) enable

determination of chemical composition and proposed structural assignment of glycolipids and phospholipids. High mass

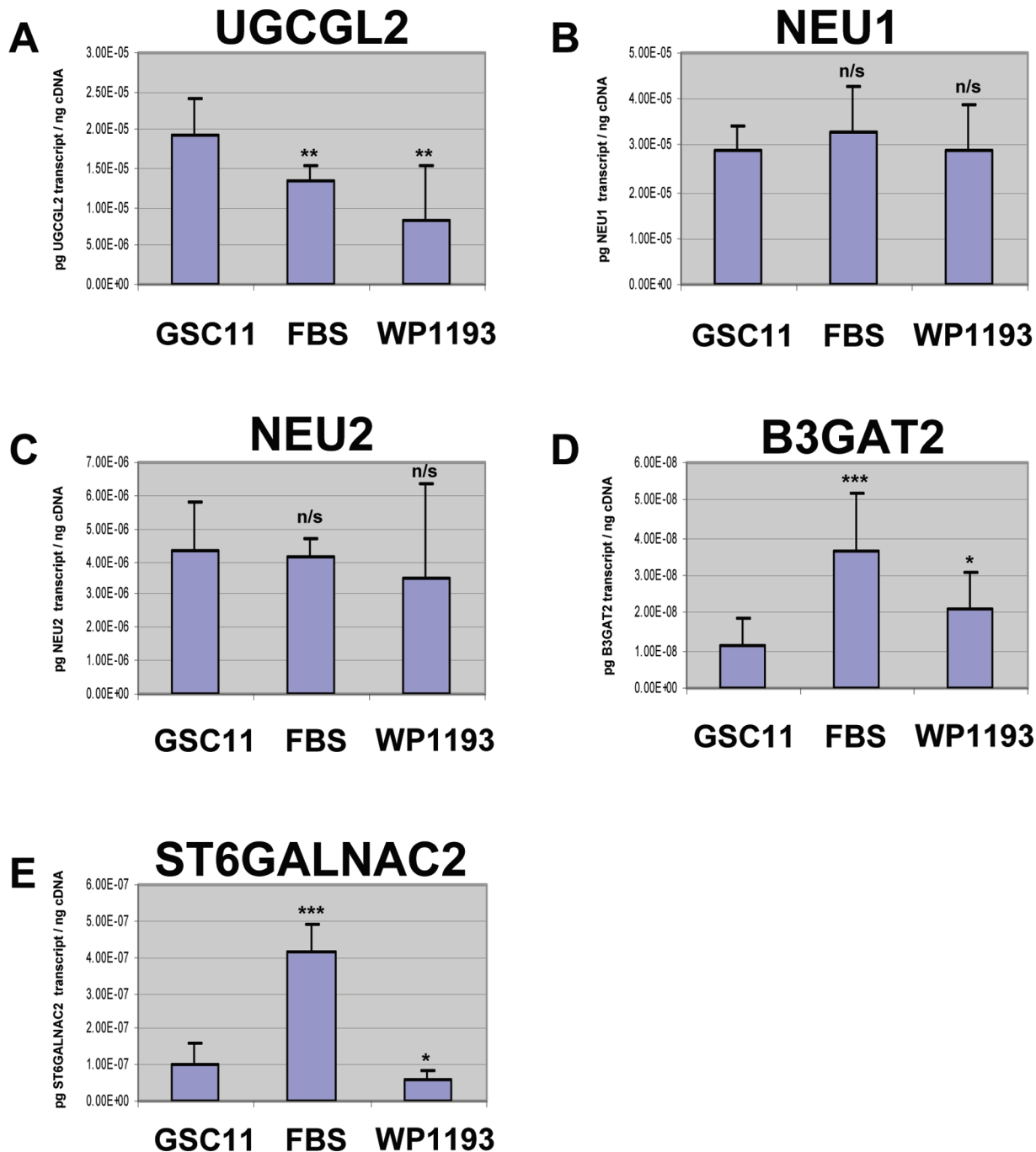


**Figure 2.** qRT-PCR corroboration of selected glyco-targets identified by microarray analysis. For each mRNA, transcript abundance, normalized to cDNA, was calculated by qRT-PCR, as described in Experimental Procedures. Data are presented for UGCGL2 (A), NEU1 (B), NEU2 (C), B3GAT2 (D) and ST6GALNAC2 (E) and represent mean ( $\pm$ SD). Significant differences from control GSC11 cells for all genes assessed by two-tailed, unpaired Student's *t* test (\* $p$  < 0.05, \*\* $p$  < 0.01, \*\*\* $p$  < 0.001). n/s, not significant ( $p$  > 0.05).

accuracy and high resolving power of high-field FT-ICR mass spectrometry<sup>38,39,41,42</sup> greatly improved the resolution and assignment of glycolipids and phospholipids in the complex mixture of polar lipid extracts from GSC11 cells.

We detected seven major glycolipid subclasses, including 13 GM3 isoforms, 21 GM2 $\alpha$ , 10 GM1b, 6 GD2, 4 O-acetyl-GD2, 18 GD1 and 6 asialo-GM1. Tandem mass spectra generated from collisional induced dissociation (CID) of precursor ions in the linear ion trap (LTQ) suggest that major isomers are GM2 $\alpha$  (with trace GM2) and GM1b (trace GM1 and GM1 $\alpha$ ). Notation inside the parentheses indicates the ceramide structure. For

example, GM3 (d34:1) represents GM3 species with 2 hydroxyl groups, 34 total carbons and 1 double bond in the ceramide tail.

Glycolipid levels underwent significant changes following FBS treatment of GSC11 cancer stem cells. We detected a general increase of glycosphingolipids, including GM2 $\alpha$  (Figure 3, top left), GD2 and O-acetyl-GD2 (Figure 3, top right), asialo-GM1 (Figure 3, bottom left), GM1b (Figure 3, bottom middle) and GM3 (Figure 3, bottom right). The only exception is GD1 (Supplementary Table 1) which remains stable after serum

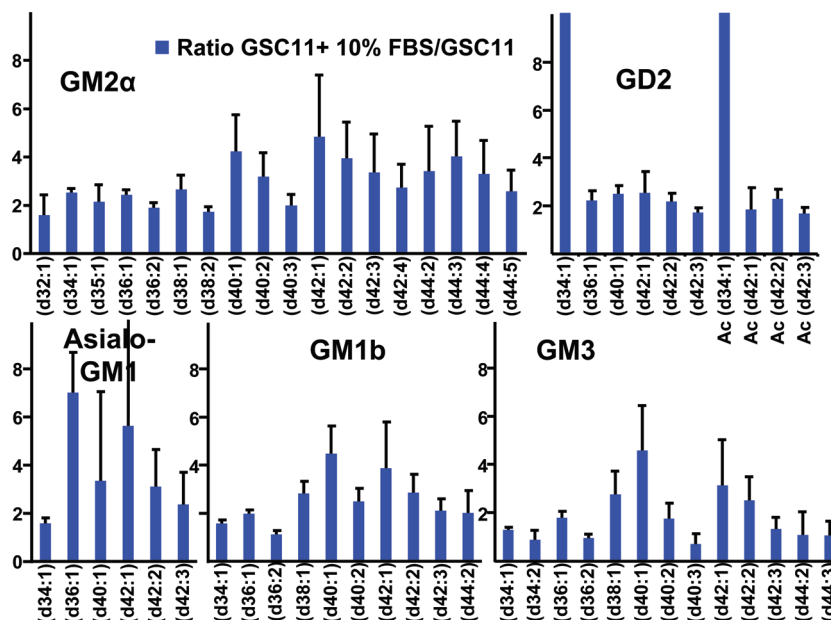


**Figure 3.** Ratio of signal magnitudes (based on FT-ICR mass spectral peak height) of various glycolipid ions with vs without serum treatment of GSC11. Error bars reflect the standard deviation of a total six replicates (two biological replicates with three analytical replicates each). Note the general increase in glycosphingolipids, including GM2 $\alpha$ , GD2, O-acetyl-GD2 (Ac-GD2), asialo-GM1, GM1b, and GM3.

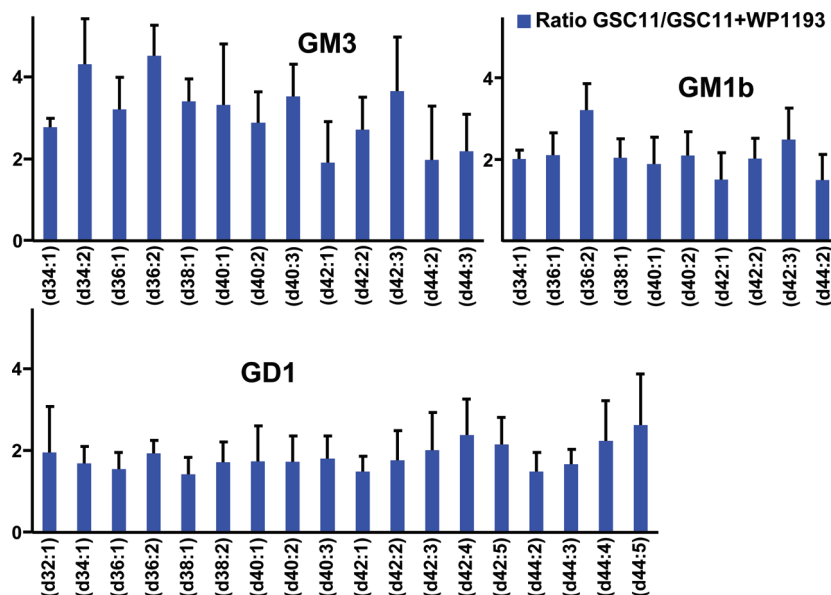


**Figure 4.** Effect of STAT3 phosphorylation inhibition (with WP1193) of GSC11 on glycolipid composition, displayed as in Figure 3.

treatment. Such change results in a general increase of cell surface sialic acid presented by glycosphingolipids.

When GSC11 cells were treated with WP1193, a STAT3 phosphorylation inhibitor, we observed decreases in a few glycosphingolipids, including GM3 (Figure 4, top left), GM1b (Figure 4, top right) and GD1 (Figure 4, bottom). Levels of other glycosphingolipids, including GM2 $\alpha$ , GD2, O-acetyl-GD2, and asialo-GM1, remain stable (Supplementary Table 1). Such changes decrease the cell surface glycans presented by glycosphingolipids.

The combination of MS techniques with high mass accuracy (FT-ICR MS) and high sensitivity and fast duty cycle (LTQ MS $^n$ ) enable us to predict newly identified glycolipid structures. For example, we observed doubly charged ions,  $[M - 2H]^{2-}$ ,  $m/z$  899.5045, 42.0094 Da higher in mass than GD2 (d42:1),  $[M -$

$2H]^{2-}$ ,  $m/z$  878.4998. The increase in mass may be due to addition of an acetyl group (chemical formula  $C_2H_2O$ , mass = 42.0106 Da). Comparison of tandem mass spectra for these two ion species (Figure 5) shows the same mass fragments due to the loss of a terminal sugar residue (Figure 5, blue dotted line). The two sets of fragments that contain terminal sialic acid (Figure 5, red dotted lines) show a mass shift of 42 Da, indicating that the acetyl group is located on the terminal sialic acid of the GD2 species.

**Identification of 3-Sulfoglucuronylparagloboside.** We identified an acidic glycolipid species that is most likely 3-sulfoglucuronylparagloboside. A tandem mass spectrum of a representative 3-sulfoglucuronylparagloboside (d42:2) is shown in Figure 6. Characteristic neutral loss of 80 Da in the LTQ tandem mass spectrum (Figure 6), high mass accuracy (<1 ppm) of the

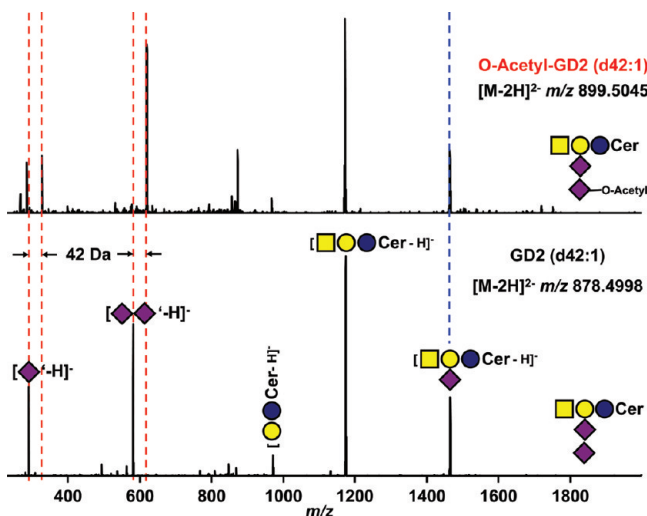


**Figure 5.** LTQ tandem mass spectra of GD2 and O-acetyl-GD2. Bottom, GD2; top, O-acetyl-GD2. Fragments without the terminal sialic acid are indicated by a blue dotted line. Fragments including terminal sialic acid are indicated by red dotted lines: note the 42 Da mass increases for these fragments in O-acetyl-GD2.

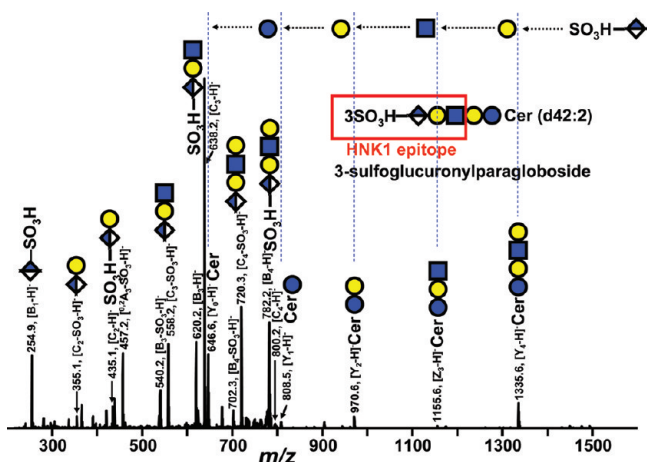


**Figure 6.** LTQ tandem mass spectrum of 3-sulfoglucuronylparagloboside (d42:2). The ceramide backbone contains 2 hydroxyl groups, 42 total carbons, and 2 double bonds. Precursor ions are doubly deprotonated,  $[M - 2H]^{2-}$ ,  $m/z$  795.4171. The HNK1 epitope, containing 3-sulfoglucuronic acid attached to lactosamine, is highlighted in a red box. Sequential loss of sugar residues verifies the proposed glycoform sequence. Nomenclature of fragment products follows a prior literature report.<sup>50</sup>

precursor ions, isotopic fine structure for sulfur speciation and a 9.4 T FT-ICR Infrared multiphoton dissociation (IRMPD) tandem mass spectrum (data not shown) confirm the glycan sequence and support a linear linkage. This class of sulfated glycolipid was found to be up-regulated in serum treated GSC11 and down-regulated by STAT3 phosphorylation inhibition.

**Phospholipids.** Phospholipids are the major components of the cell membrane, and their compositions and modifications affect the membrane fluidity and phospholipid-mediated signaling pathways. Four classes of phospholipids including phosphatidylinositol (PI), phosphatidylethanolamine (PE), phosphatidylcholine (PC) and sphingomyelin (SM) were detected. Hydroxylation of the acyl groups was minimal. Because PC and SM contain terminal choline (2-hydroxyethyl trimethylammonium) with a quaternary ammonium cation (positive charge on nitrogen), PC and SM negative ions were detected as

adducts with counterions (acetate, formate and occasionally chloride). The reported signal magnitudes of PC and SM were the sum of all the detected adducts.

LC retention time can be used to differentiate between isomers. For example, singly deprotonated ions,  $[M - H]^{1-}$ , with  $m/z$  871.6922 were assigned as SM (d42:2) acetate adduct based on accurate mass and tandem mass spectra. Another singly charged ion,  $[M - H]^{1-}$ , with  $m/z$  857.6757 was detected with the same retention time and could be SM (d42:2) formate adduct or SM (d41:2) acetate adduct. On the basis of our previous observation that fewer total carbons in the ceramide tails lead to a shorter retention time relative to longer-chain ceramides,<sup>33</sup> we assigned the  $[M - H]^{1-}$ ,  $m/z$  857.6757<sup>-</sup> species as an SM (d42:2) formate adduct. Comparison of tandem mass spectra also confirmed the assignment.<sup>34</sup>

Following FBS treatment, notable changes in the phospholipid profile were observed (Figure 7). PI levels of longer chain and more unsaturated (containing more double bonds in the diacyl chains) species increased (Figure 7, top) and so did PE (Supplementary Table 1). For example, increase (ratio) of PI (40:6) and (40:7) is much higher than that of (40:3) and (40:4).

PC species show expression patterns (Figure 7, bottom left) different from those of PI and PE. A general increase in the PC levels not affected by unsaturation (double bonds) was observed. Interestingly, PC preferentially expressed shorter diacyl [for example, PC (34:1)] species, whereas PI and PE preferentially expressed longer diacyl [for example, PI (38:4) species. FBS treated GSC11 cells also showed higher levels of SM (Figure 7, bottom right), especially short chain SM. For example, short chain SM (including [d34:1], [d34:2], [36:1] and [36:2]) shows higher increase (ratio) than long chain SM (including [d42:1], [d42:2] and [d42:3]). When GSC11 cells were treated with the STAT3 phosphorylation inhibitor, phospholipid levels were relatively stable (Supplementary Table 1).

## Discussion

The aberrant cell surface glycosylation patterns present on virtually all tumors have been linked to altered cellular morphology, oncogenic transformation, tumor progression, metastasis, and invasivity. Altered cell surface glycosylation patterns in glioblastoma detected by an oligonucleotide microarray platform that represented all of the cloned human glycogenes (i.e., glycosidases, glycosyltransferases, polysaccharide lyases, carbohydrate esterases, and carbohydrate-binding proteins) have been previously characterized.<sup>30</sup>

Our focused microarray<sup>30</sup> deserves further elaboration. The quality of our platform has been rigorously evaluated in terms of dynamic range, discrimination power, accuracy, reproducibility and specificity. The ability to reliably measure even low levels of statistically significant differential gene expression stems from coupling (a) stringently designed and quality controlled chip manufacturing and transcript labeling protocols, (b) rigorous data analysis algorithms, and (c) flexible ontological and interactome analyses capable of demonstrating significant correlations between the expression of specific genesets. When combined with robust qRT-PCR corroboration, this approach provides a very powerful platform to identify fundamental, biologically relevant cellular pathways significantly altered in human stem cells.

For serum-exposed GSC11 cells, we observed a general increase of cell surface sialic acids present on glycosphingolipids. Increase of GM3, GM2 $\alpha$ , GD2, O-acetyl-GD2 and GM1b may be due to a 4-fold increase of transcripts for ST6GALNAC2

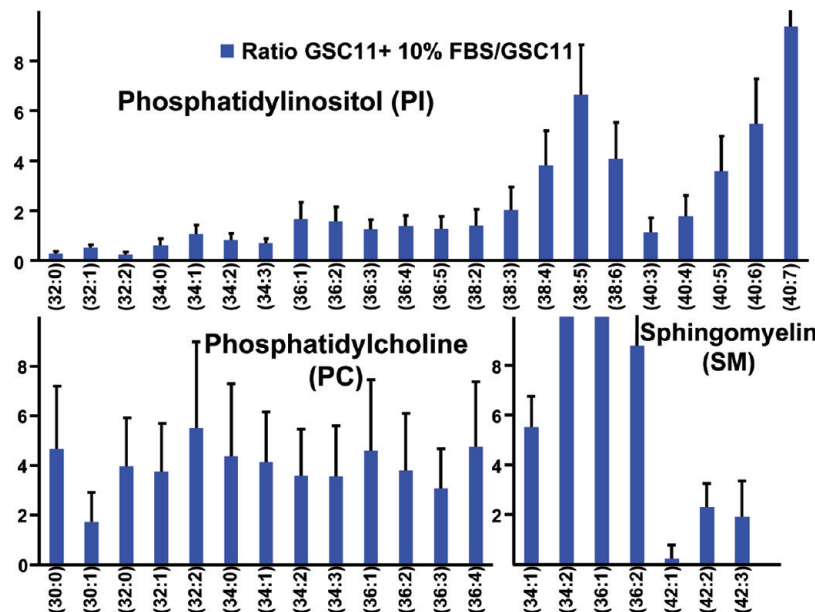


**Figure 7.** Effect of serum treatment of GSC11 on phospholipid composition, displayed as in Figure 3. PC (phosphatidylcholine) shows general increases, whereas PI (phosphatidylinositol) shows increase of longer and more unsaturated (containing more double bonds) species after FBS treatment. SM (sphingomyelin) shows a preferred increase of short chain species.

as reported in qRT-PCR. ST6GALNAC2 gene encodes a sialyltransferase which can transfer sialic acids to glycosphingolipids. qRT-PCR verified a decrease of UGCGL2, a gene for glucosylceramide synthase (GCS). This enzyme catalyzes the formation of glucosylceramide (GlcCer) from ceramide in the initial step of ganglioside biosynthesis. Although the reduced transcript of UGCGL2 may lead to a decrease of glycosphingolipid precursors, much higher increase of transcript for sialyltransferase may compensate for this effect. Up-regulation of 3-sulfoglucuronylparagloboside carrying an HNK1 epitope (Figure 6) may correlate to increased transcripts of B3GAT1 (verified by qRT-PCR), a gene that encodes the glucuronosyltransferase involved in biosynthesis of the HNK1 glycan.<sup>43,44</sup>

Changes in phospholipid composition not only modulate the membrane fluidity, but also affect the phospholipid-mediated signal transduction. For example, phosphorylated PI, including inositol 3,4-bisphosphate [PI(3,4)P<sub>2</sub>] and inositol 3,4,5-triphosphate [PI(3,4,5)P<sub>3</sub>], affected cell proliferation, survival, and movement.<sup>45</sup> Presence of a double bond results in a "kink" in the phospholipid fatty acyl chain. Thus, differentiated tumor cells with a higher ratio of unsaturated phospholipids may result in a more fluid cell membrane because phospholipids with more double bonds pack much more loosely than those with fewer double bonds. More differentiated tumor cells also show an increase in PC and SM, which are predominantly localized on the outer plasma membrane and carry positive charges.<sup>46</sup> Taken together with the increase in cell surface glycans present on glycolipids, such dramatic modulation in cell surface charge and glycan composition is likely to affect the intercellular signal transduction and the intracellular pathways.

In WP1193-treated cells, the decrease of glycosphingolipids, including GM3, GM1b and GD1 might be due to a combined decrease of transcripts for UGCGL2, and ST6GALNAC2. As discussed earlier, reduced transcripts of UGCGL2 may result in reduced precursor (GlcCer) for glycosphingolipid synthesis. Reduced ST6GALNAC2 may lead to reduced sialyltransferase activities toward synthesizing sialic acid containing glycosph-

ingolipids. As for the decreased surface glycans presented by glycosphingolipids, decreased glycoprotein levels were also noted in the STAT3 phosphorylation inhibited GSC11 cells (data not shown). In response to STAT3 phosphorylation inhibition, decreased levels of cell surface glycans on glycolipids and glycoproteins can change the cell surface charge and inevitably affect adhesion and cellular cross-talk.

In a recent report on rat and murine brain microglial cells, treatment with GM1 or GD1a led to rapid and transient phosphorylation of STAT3 as well as STAT1.<sup>47</sup> Presence of sialic acid proved to be crucial for such modulation. Treatment with asialo-GM1, a glycolipid with one less sialic acid than GM1, did not induce phosphorylation of STAT. However, treatment of GSC11 cells with asialo-GM1 did reduce the levels of galectin-1 in a dose-dependent fashion (unpublished data).

A quantitative phosphoproteomic study on the response of STAT3 phosphorylation inhibition of GSC11 cells was recently reported.<sup>48</sup> One of the most highly upregulated phosphoproteins was identified as ANK2. ANK2 can bind to several cell adhesion molecules carrying HNK1 carbohydrate (Figure 6) which is also contained in 3-sulfoglucuronylparagloboside. Three enzymes, including GANAB, RPNI and STT3B, related to N-glycan synthesis, were found to be upregulated. HEXB (hexosaminidase B), an enzyme that degrades glycosphingolipids in the lysosome, was found modulated by STAT3 phosphorylation inhibition. A 1.7-fold decrease of HEXB was observed in the phosphoproteomic data set<sup>48</sup> and a 1.11-fold decrease in HEXB transcripts was observed in the current study (Table 2). Moreover, seven proteins that regulate nitric oxide synthase 2 (NOS2, also named inducible NOS, iNOS) were found to be upregulated and upregulation of iNOS was confirmed by Western blot.<sup>48</sup> Inducible NOS interacts directly with cav-1, a protein enriched in detergent-insoluble membrane fraction (or "lipid raft", which is highly enriched in cholesterol and glycosphingolipids).<sup>49</sup> In human colon carcinoma cells, cav-1 down-regulates NO production by recruiting iNOS to the "lipid raft" where iNOS is subject to proteolytic degradation.<sup>49</sup> In response to STAT3 phosphorylation inhibition, changes of

composition of glycosphingolipids may lead to modulation of the microenvironment of lipid rafts, which potentially could affect the regulation of iNOS. These preliminary findings will require future study, but demonstrate the use of systems-wide studies to generate new biological hypotheses.

Overall, these results demonstrate that alterations in differentiation or self-renewal states of glioma stem cells results in significant changes in discrete biochemical pathways that modulate the expression of cell surface glycoconjugates and phospholipids. Moreover, these changes may provide a foundation for studies that will aid in the definition of the molecular basis for glioma stem cell maintenance and tumorigenesis. A systems biology approach employing lipidomics, transcriptomics, and proteomics generates new biological hypotheses for future research targeting CSCs.

**Abbreviations:** EGF, epidermal growth factor; bFGF, basic fibroblast growth factor; STAT3, signal transducer and activator of transcription 3; HNK1, human natural killer-1; NEU1, sialidase 1 (lysosomal sialidase); CD133, prominin 1; ST6GALNAC2, ST6-( $\alpha$ -N-acetyl-neuraminy1-2,3- $\beta$ -galactosyl-1,3)-N-acetylgalactosaminide  $\alpha$ 2,6-sialyltransferase2; UGCGL2, UDP-glucose ceramide glucosyltransferase-like 2; FBS, fetal bovine serum; B3GAT1,  $\beta$ 1, 3-glucuronyltransferase 1; CSC, cancer stem cell; FT-ICR MS, Fourier Transform Ion Cyclotron Resonance Mass Spectrometry; ESC, embryonic stem cell; GSL, glycosphingolipid; SLe<sup>x</sup>, sialyl-lewis<sup>x</sup>; SLe<sup>a</sup>, sialyl-lewis<sup>a</sup>; CFU, serial colony-forming unit; DMSO, dimethyl sulfoxide; HEPES, 4-(2-hydroxyethyl)-1-piperazineethanesulfonic acid; LOWESS, locally weighted scatterplot smoothing; nLC-MS, nanoliquid chromatography mass spectrometry; PIGA, phosphatidylinositol glycan; HEXA, hexosaminidase A; GLA, alpha galactosidase; ECM, Extracellular Matrix; GLB1,  $\beta$ 1-galactosidase; C1GALT1, core 1 synthase, glycoprotein-N-acetylgalactosamine 3- $\beta$ -galactosyltransferase 1; POMT2, protein-O-mannosyltransferase 2; MGAT2, mannosyl ( $\alpha$ 1,6)-glycoprotein  $\beta$ 1,2-N-acetylglicosaminyltransferase, MGAT4B, mannosyl ( $\alpha$ 1,3)-glycoprotein  $\beta$ 1,4-N-acetylglicosaminyltransferase, isozyme B; DPM1, dolichyl-phosphate mannosyltransferase polypeptide 1; B3GNT1, UDP-GlcNAc:  $\beta$ Gal  $\beta$ 1,3-N-acetylglicosaminyltransferase 1; UGT1A1, UDP glucuronyltransferase A1; LTQ, linear quadrupole ion trap; qRT-PCR, quantitative real time polymerase chain reaction.

**Acknowledgment.** Financial support from the NSF Division of Materials Research through DMR-06-54118, the State of Florida, and the CERN Foundation, Dr. Marnie Rose Foundation, John C. Merchant Memorial Fund, and the Falk Foundation (Chicago, IL) is gratefully acknowledged.

**Supporting Information Available:** Supplementary Table 1 Glycolipids and phospholipids identified in baseline and treated GSC11 cells. This material is available free of charge via the Internet at <http://pubs.acs.org>.

## References

- Clarke, M. F.; Dick, J. E.; Dirks, P. B.; Eaves, C. J.; Jamieson, C. H.; Jones, D. L.; Visvader, J.; Weissman, I. L.; Wahl, G. M. Cancer stem cells - Perspectives on current status and future directions: AACR Workshop on Cancer Stem Cells. In: *Cancer Res.* **2006**, *66*, 9339-9344.
- Vlashi, E.; McBride, W. H.; Pajonk, F. Radiation responses of cancer stem cells. *J. Cell. Biochem.* **2009**, *108* (2), 339-342.
- Hakomori, S. Tumor malignancy defined by aberrant glycosylation and sphingo(glyco)lipid metabolism. *Cancer Res.* **1996**, *56* (23), 5309-5318.
- Hakomori, S. Glycosylation defining cancer malignancy: new wine in an old bottle. *Proc. Natl. Acad. Sci. U.S.A.* **2002**, *99* (16), 10231-10233.
- Muramatsu, T. Carbohydrate signals in metastasis and prognosis of human carcinomas. *Glycobiology* **1993**, *3* (4), 291-296.
- Hakomori, S.; Igarashi, Y. Functional role of glycosphingolipids in cell recognition and signaling. *J. Biochem.* **1995**, *118* (6), 1091-1103.
- Chatterjee, S.; Wei, H. Roles of glycosphingolipids in cell signaling: adhesion, migration, and proliferation. *Methods Enzymol.* **2003**, *363*, 300-312.
- Yamashita, T.; Wada, R.; Sasaki, T.; Deng, C.; Bierfreund, U.; Sandhoff, K.; Proia, R. L. A vital role for glycosphingolipid synthesis during development and differentiation. *Proc. Natl. Acad. Sci. U.S.A.* **1999**, *96* (16), 9142-9147.
- Hakomori, S.; Handa, K.; Iwabuchi, K.; Yamamura, S.; Prinetti, A. New insights in glycosphingolipid function: "glycosignaling domain," a cell surface assembly of glycosphingolipids with signal transducer molecules, involved in cell adhesion coupled with signaling. *Glycobiology* **1998**, *8* (10), xi-xix.
- Simons, K.; Toomre, D. Lipid rafts and signal transduction. *Nat. Rev. Mol. Cell Biol.* **2000**, *1* (1), 31-39.
- Ono, M.; Hakomori, S. Glycosylation defining cancer cell motility and invasiveness. *Glycoconjugal J.* **2004**, *20* (1), 71-78.
- Ono, M.; Handa, K.; Withers, D. A.; Hakomori, S. Glycosylation effect on membrane domain (GEM) involved in cell adhesion and motility: a preliminary note on functional alpha3, alpha5-CD82 glycosylation complex in ldlD 14 cells. *Biochem. Biophys. Res. Commun.* **2000**, *279* (3), 744-750.
- Taieb, N.; Maresca, M.; Guo, X. J.; Garmy, N.; Fantini, J.; Yahia, N. The first extracellular domain of the tumour stem cell marker CD133 contains an antigenic ganglioside-binding motif. *Cancer Lett.* **2009**, *278* (2), 164-173.
- Jiang, H.; Gomez-Manzano, C.; Aoki, H.; Alonso, M. M.; Kondo, S.; McCormick, F.; Xu, J.; Bekele, B. N.; Colman, H.; Lang, F. F.; Fueyo, J. Examination of the therapeutic potential of delta-24-RGD in brain tumor cells: Role of autophagic cell death. *J. Natl. Cancer Inst.* **2007**, *99*, 1410-1414.
- Potten, C. S.; Owen, G.; Booth, D. Intestinal stem cells protect their genome by selective segregation of template DNA strands. *J. Cell Sci.* **2002**, *115*, 2381-2388.
- Vlashi, E.; McBride, W. H.; Pajonk, F. Radiation responses of cancer stem cells. *J. Cell. Biochem.* **2009**, *108* (2), 339-342.
- Bez, A.; Corsini, E.; Curti, D.; Biggiogera, M.; Colombo, A.; Nicosia, R. F.; Pagano, S. F.; Parati, E. A. Neurosphere and neurosphere-forming cells: morphological and ultrastructural characterization. *Brain Res.* **2003**, *993*, 18-29.
- Reynolds, B. A.; Weiss, S. Generation of neurons and astrocytes from isolated cells of the adult mammalian central nervous system. *Science* **1992**, *255* (5052), 1707-1710.
- Baumann, M.; Krause, M.; Thames, H.; Trott, K.; Zips, D. Cancer stem cells and radiotherapy. *Int. J. Radiat. Biol.* **2009**, *85* (5), 391-402.
- Reynolds, B. A.; Tetzlaff, W.; Weiss, S. A multipotent EGF-responsive striatal embryonic progenitor cell produces neurons and astrocytes. *J. Neurosci.* **1992**, *12* (11), 4565-4574.
- Shmelkov, S. V.; St.Clair, R.; Lyden, D.; Rafii, S. AC133/CD133/Prominin-1. *Int. J. Biochem. Cell Biol.* **2005**, *37* (4), 715-719.
- Singh, S. K.; Clarke, I. D.; Terasaki, M.; Bonn, V. E.; Hawkins, C.; Squire, J.; Dirks, P. B. Identification of a cancer stem cell in human brain tumors. *Cancer Res.* **2003**, *63* (18), 5821-5828.
- Wang, J.; Sakariassen, P. O.; Tsinkalovsky, O.; Immervoll, H.; Bøe, S. O.; Svendsen, A.; Prestegarden, L.; Røslund, G.; Thorsen, F.; Stuhr, L.; Molven, A.; Bjerkvig, R.; Enger, P. Ø. CD133 negative glioma cells form tumors in nude rats and give rise to CD133 positive cells. *Int. J. Cancer* **2008**, *122*, (4), 761-768.
- Zheng, X.; Shen, G.; Yang, X.; Liu, W. Most C6 cells are cancer stem cells: evidence from clonal and population analyses. *Cancer Res.* **2007**, *67* (8), 3691-3697.
- Embryonic Stem Cell Protocols: Differentiation Models*, 2nd ed.; Turkson, K., Ed.; Humana Press: Totowa, NJ, 2006; Vol. 2.
- Balasubramaniyan, V.; Bhat, K. P.; Wang, S.; Vaillant, B.; Gumin, J.; Sai, K.; Kim, S. H.; Lang, F.; Bogler, O.; Aldape, K.; Colman, H. Tumorigenicity is independent of differentiation in glioblastoma stem cells, manuscript in preparation.
- Heimberger, A. B.; Priebe, W. Small molecule inhibitors of p-STAT3: novel agents for treatment of primary and metastatic CNS cancers. *Recent Pat. CNS Drug Discovery* **2008**, *3* (13), 179-188.
- Haura, E. B.; Turkson, J.; Jove, R. Mechanisms of disease: Insights into the emerging role of signal transducers and activators of transcription in cancer. *Nat. Clin. Pract.* **2005**, *2* (6), 315-323.

- (29) Bromberg, J. F.; Wrzeszczynska, M. H.; Devgan, G.; Zhao, Y.; Pestell, R. G.; Albanese, C.; Darnell, J. E., Stat3 as an Oncogene. *Cell* **1999**, *99* (2), 238–239.
- (30) Kroes, R. A.; Dawson, G.; Moskal, J. R. Focused microarray analysis of glyco-gene expression in human glioblastomas. *J. Neurochem.* **2007**, *103* (Suppl. 1), 14–24.
- (31) Lee, P. D.; Sladek, R.; Greenwood, C. M.; Hudson, T. J. Control genes and variability: absence of ubiquitous reference transcripts in diverse mammalian expression studies. *Genome Res.* **2002**, *12* (2), 292–297.
- (32) Kroes, R. A.; Panksepp, J.; Burgdorf, J.; Otto, N. J.; Moskal, J. R. Modeling depression: Social dominance-submission gene expression patterns in rat neocortex. *Neuroscience* **2006**, *137* (1), 37–49.
- (33) He, H.; Conrad, C. A.; Nilsson, C. L.; Ji, Y.; Schaub, T. M.; Marshall, A. G.; Emmett, M. R. Method for Lipidomic Analysis: p53 Expression Modulation of Sulfatide, Ganglioside, and Phospholipid Composition of U87 MG Glioblastoma Cells. *Anal. Chem.* **2007**, *79* (22), 8423–8430.
- (34) He, H.; Nilsson, C. L.; Emmett, M. R.; Ji, Y.; Marshall, A. G.; Kroes, R. A.; Moskal, J. R.; Schmidt, M.; Colman, H.; Lang, F. F.; Conrad, C. A. Cellular Glycolipids in Cultured Glioblastoma Multiforme Brain Tumor Cells, Sanibel Conference on Mass Spectrometry-Lipidomics and Lipids in Mass Spectrometry, St. Petersburg Beach, FL, January 23–26, 2009.
- (35) He, H.; Nilsson, C. L.; Emmett, M. R.; Ji, Y.; Marshall, A. G.; Kroes, R. A.; Schmidt, M.; Moskal, J. R.; Colman, H.; Lang, F. F.; Conrad, C. A. Polar lipid remodeling and increased sulfatide expression are associated with the glioma therapeutic candidates, wild type p53 elevation and the topoisomerase-1 inhibitor, Irinotecan. *Glycoconjugate J.* **2010**, *27*, 27–28.
- (36) Emmett, M. R.; Caprioli, R. M. Microelectrospray mass spectrometry: ultra-high-sensitivity analysis of peptides and proteins. *J. Am. Soc. Mass Spectrom.* **1994**, *5*, 605–613.
- (37) Emmett, M. R.; White, F. M.; Hendrickson, C. L.; Shi, S. D.; Marshall, A. G. Application of micro-electrospray liquid chromatography techniques to FT-ICR mass spectrometry to enable high-sensitivity biological analysis. *J. Am. Soc. Mass Spectrom.* **1998**, *9*, 333–340.
- (38) Schaub, T. M.; Blakney, G. T.; Hendrickson, C. L.; Quinn, J. P.; Senko, M. W.; Marshall, A. G. LC/MS, Proteins, and Petroleum: Performance Characteristics of a 14.5 T LTQ FT-ICR Mass Spectrometer. 55th Meeting of the American Society for Mass Spectrometry, Indianapolis, IN, June 3–7, 2007.
- (39) Schaub, T. M.; Hendrickson, C. L.; Horning, S.; Quinn, J. P.; Senko, M. W.; Marshall, A. G. High performance mass spectrometry: Fourier transform ion cyclotron resonance at 14.5 Tesla. *Anal. Chem.* **2008**, *80*, 3985–3990.
- (40) Levery, S. B. Glycosphingolipids structural analysis and glycosphingolipidomics. *Methods Enzymol.* **2005**, *405*, 300–369.
- (41) Marshall, A. G.; Hendrickson, C. L.; Jackson, G. S. Fourier transform ion cyclotron resonance mass spectrometry: a primer. *Mass Spectrom. Rev.* **1998**, *17*, 1–35.
- (42) Senko, M. W.; Hendrickson, C. L.; Emmett, M. R.; Shi, S. D.-H.; Marshall, A. G. External accumulation of ions for enhanced electrospray ionization Fourier transform ion cyclotron resonance mass spectrometry. *J. Am. Soc. Mass Spectrom.* **1997**, *8* (970–976), 970.
- (43) Kizuka, Y.; Matsui, T.; Takematsu, H.; Kozutsumi, Y.; Kawasaki, T.; Oka, S. Physical and functional association of glucuronyltransferases and sulfotransferase involved in HNK-1 biosynthesis. *J. Biol. Chem.* **2006**, *281* (19), 13644–13651.
- (44) Mitsumoto, Y.; Oka, S.; Sakuma, H.; Inazawa, J.; Kawasaki, T. Cloning and chromosomal mapping of human glucuronyltransferase involved in biosynthesis of the HNK-1 carbohydrate epitope. *Genomics* **2000**, *65* (2), 166–173.
- (45) Di Paolo, G.; De Camilli, P. Phosphoinositides in cell regulation and membrane dynamics. *Nature* **2006**, *443*, 651–657.
- (46) Yamaji-Hasegawa, A.; Tsujimoto, M. Asymmetric distribution of phospholipids in biomembranes. *Biol. Pharm. Bull.* **2006**, *29* (8), 1547–1553.
- (47) Kim, O. S.; Park, E. J.; Joe, E.-h.; Jou, I. JAK-STAT Signaling mediates gangliosides-induced inflammatory responses in brain microglial cells. *J. Biol. Chem.* **2002**, *277* (43), 40594–40601.
- (48) Nilsson, C. L.; Dillon, R.; Devakumar, A.; Shi, D.-H.; Greig, M.; Rogers, J. C.; Krastins, B.; Rosenblatt, M.; Kilmer, G.; Major, M.; Kaboord, B. J.; Sarracino, D.; Rezai, T.; Prakash, A.; Lopez, M.; Ji, Y.; Priebe, W.; Lang, F. F.; Colman, H.; Conrad, C. A. Quantitative phosphoproteomic analysis of the STAT3/IL-6/HIF1alpha signaling network: an initial study in GSC11 glioblastoma stem cells. *J. Proteome Res.* **2010**, *9* (1), 430–443.
- (49) Felley-Bosco, E.; Bender, F. C.; Courjault-Gautier, F.; Bron, C.; Quest, A. F. Caveolin-1 down-regulates inducible nitric oxide synthase via the proteasome pathway in human colon carcinoma cells. *Proc. Natl. Acad. Sci. U.S.A.* **2000**, *97* (26), 14334–14339.
- (50) Domon, B.; Costello, C. E. A systematic nomenclature for carbohydrate fragmentations in FAB-MS/MS spectra of glycoconjugates. *Glycoconjugate J.* **1998**, *5* (4), 397–409.

PR900793A